

STRONG GROUND MOTIONS DURING THE 2011 PACIFIC COAST OFF TOHOKU, JAPAN EARTHQUAKE

Kojiro IRIKURA¹ and Susumu KURAHASHI²

¹ Professor, Disaster Prevention Research Center, Aichi Institute of Technology,
Toyota, Japan, irikura@geor.or.jp

² Lecturer, Disaster Prevention Research Center, Aichi Institute of Technology,
Toyota, Japan, susumu@aitech.ac.jp

ABSTRACT: The 2011 Tohoku Earthquake occurred along the plate boundary east of northeastern Japan. Huge tsunami caused tremendous disasters near the Pacific coast of northeastern Japan. In addition, strong ground motions affected ground failures, then causing liquefaction, subsequently infrastructure and building damage over soft-ground areas. Slip and moment rate distributions were inverted using long-period strong motion data (20 – 200 sec). Very large slip was obtained on the shallower part of the fault plane. Large peak moment rate was shown on deeper part as well as on shallower part. The source model for generating short-period motions was estimated from short-period strong motion data. The acceleration records at stations show several isolated wave-packets arriving from different origins on the source fault. Such origins are considered to be the strong motion generation areas (SGMA). We identified five wave-packets in the observed seismograms, which were arriving from five SMGAs on the source fault. The source model is estimated from the forward modeling, comparing short-period ground motions simulated using the empirical Green's functions with those observed. The final model has five SMGAs over the source fault located west of the hypocenter and along the down-dip edge of the source fault. Attenuation-distance relationship of peak ground velocity (PGV) from this earthquake was virtually equivalent to the empirical one from Mw 8.0 determined by Si and Modorikawa (1999). On the other hand, peak ground acceleration (PGA) was also virtually equivalent to the empirical one from Mw 8.0 in the distance over 100 km, but clearly larger than that from Mw 8.0 near the source fault. Ground motions with extremely high-accelerations can be explained by two different causes. One is nonlinear site responses due to surface geology with decreased S wave velocities (nonlinear soil behavior). The other is source characteristics, such as rupture directivity effects, heterogeneous slip velocity inside the strong motion generation areas and so on. Very little damage during this earthquake is explained by spectral characteristics of ground motions with predominant periods shorter than 0.5 sec, although accelerations were so high.

Key Words: 2011 Tohoku earthquake, strong ground motions, strong motion generation area, characterized source model, attenuation-distance relationship

INTRODUCTION

The 11 March 2011 giant earthquake with Mw 9.0 occurred off the Pacific coast of Tohoku, and is the largest historical earthquake to strike in or near Japan. The rupture was initiated approximately 100 km off-shore of Miyagi prefecture and extended about 450 km in length and about 200 km in width along the subducting Pacific plate. The focal mechanism showed a reverse fault with a compression axis in a WNW-ESE direction.

The huge tsunami generated by this earthquake struck the east-coast along Tohoku, resulting in more than 19,000 people being killed or missing. The tsunami waves were also responsible for severe accidents at the nuclear reactors in the Fukushima Daiichi Nuclear Power Plant, which further intensified the scope of the disaster.

Strong ground motions with high seismic intensity such as 6-upper and 6-lower in the JMA scale extends from the Tohoku to the Kanto district, over an area of about 400 km × 100 km (Hoshiba et al., 2011). A maximum seismic intensity 7 (corresponding to greater than 10 on the Modified Mercalli scale) was recorded at Tsukidate (MYG004) in Kurihara about 175 km from the epicenter. Even at some stations in Tokyo Metropolitan area more than 350 km from the epicenter, 6-lower intensity are recorded.

More than 120 thousands houses and buildings were totally destroyed and more than 240 thousands were half collapsed. Such damaged buildings were caused mostly by tsunami. Damage by shaking was relatively less.

For the source regions of this earthquake, the Headquarters for Earthquake Research Promotion of Japan (HERP) have made long-term evaluation of seismic activity based on an idea of so-called “characteristic earthquake model” (HERP 2009a). The entire area is divided into eight regions from the seismic activity for past 400 years. For each region, the presence of characteristic earthquake was evaluated by analyzing the pattern of earthquake occurrences. For example, in offshore of Miyagi prefecture, so-called Miyagi-oki earthquakes have repeatedly occurred with almost the same size and fairly close in location each other such as the sequence of the 1936, 1978, and several other earlier events. The probability of the earthquake occurrence with M 7.4 - 7.5 is evaluated earthquake in the next 30 years is 99%. M= 7.6-7.8 at 80 % for the Southern-Sanriku-oki in the region east of the Miyagi-oki earthquake. An earthquake with M=7.3-7.5 is forecasted at less than 7 % for the Fukushima-oki and that with M=6.7-7.2, at more than 90 % for the Ibaragi-oki, respectively. The rupture of the 2011Tohoku earthquake seems to start from the source region of the Southern-Sanriku-oki earthquake which is evaluated as 80 % probability in the next 30 years.

Slip distribution models have been inverted using teleseismic, geodetic, and tsunami data by many researchers (e.g. Ide et al., 2011; Iinuma et al., 2011; Fujii and Satake, 2011; Yagi and Nishimura, 2011; Yamanaka, 2011). However, these initial modeling results exhibit significant variability, with notably dissimilar features. For example, some of the models have the main slip distribution west of the hypocenter, while others locate it east of the hypocenter toward the Japan Trench zone. The slip distributions from the tsunami data show large slip near the Trench zone. A unified source model was constructed through joint inversion of teleseismic, strong motion, and geodetic datasets by Koketsu et al. (2011) and Yokota et al. (2011). Their results showed that the main rupture propagated not only in the strike direction but also in the dip direction and included both the deep area called the Miyagi-oki region and the compact shallow area near the Japan Trench.

Strong motion data in the near-source region provide more detailed information about the shorter period rupture process during the earthquakes. In our study, we estimate a source model for generating strong ground motions from this earthquake by comparing the observed records from the mainshock with synthesized motions based on a characterized source model and the empirical Green's function method. The characterized source model consists of several strong-motion-generation-areas (SMGAs) with large slip velocity or high stress drop, distributed across the entire rupture area of the earthquake. One of features of this earthquake is relatively small damage caused by ground motions. To clarify the reasons of less damage are discussed about the characteristics of attenuation-distance relationships such as PGV and PGA in relation of the long period and short period source models.

LONG-PERIOD SOURCE MODEL

Data and Velocity-Structure Model

Long-period source model by Yishida et al. (2011) are here introduced to compare not only slip but also peak moment-rate distributions with source model for generating strong ground motions in the next section. They used the strong-motion data obtained from 37 stations of F-net and KiK-net, and 1 station (MYR, Sasatani et al., 2002) of Hokkaido University as shown in Fig. 1. These stations are located on relatively hard rock. The velocity-type broadband seismometers used for F-net (VSE-355G3) and MYR (VS3, Muramatsu et al., 2001) are very capable of recording very long-period components excited by this M 9 earthquake.

The data were windowed for 300 s, starting at P-wave arrival time, and band-pass filtered between periods of 200 s to 20 s (0.005–0.05 Hz) for waveform inversion. The accelerograms obtained from the KiK-net were integrated into ground velocities with a sampling time of 4 s.

A single fault plane was assumed for the waveform inversion analysis having a fault size, 468 km long in strike and 228 km wide in dip, referring to the aftershock distribution. The strike and dip angle were taken to be N193°E and 10°, respectively, referring to the JMA CMT solution. The rupture starting point is located at the hypocenter determined by JMA: 38.103°N, 142.861°E, 23.7 km.

The velocity structure model proposed by Wu et al. (2008, 2009) for the waveform inversion of the 1979 and 2005 Miyagi-oki earthquake was used for calculating the theoretical Green's functions. We use an identical structure model for all stations, because the stations used in the inversion are located on almost hard rock, so it is expected that the observed seismograms are less affected by local site effects in the long-period range.

Theoretical Green's functions are calculated using the discrete wavenumber method (Bouchon, 1981) and the reflection/transmission-coefficient matrix method (Kennet and Kerry, 1979) using a stratified medium. A multi-time-window linear waveform-inversion procedure (Hartzell and Heaton, 1983) was used, in which the moment-release distribution is discretized in both space and time.

To suppress instability or excessive complexity, a smoothing constraint is introduced to reduce differences in moment release values close in space. The smoothing constrained parameter used in the inversion was determined to choose the solution with a total slip which agrees with that expected from the geodetic data. Nonnegative constraints (Lawson and Hanson, 1974) to limit the rake-angle variation are also adopted, allowing to vary within 45° centered at 90°.

Slip and Peak Moment-Rate Distribution

Inversion results of total slip and peak moment rate distributions are shown in Fig. 2. Large asperity areas with large slip in the shallow part of the fault plane are remarkably seen. The asperity size is about 300 km × 100 km, and the slip on the asperity is about 20 to 47 m in Fig. 2. The slip vectors indicate an almost pure dip-slip fault mechanism. The total moment release is 4.3×10^{22} N m (M_w 9.0). This moment is similar to the seismic moment of 3.43×10^{22} N m which is derived from GPS data (Ozawa *et al.*, 2011). Synthetics calculated from the estimated rupture process agree well with compared with the observed data.

Slip models by tsunami inversion are proposed by Fujii and Satake (2011). The overall slip patterns and the average slip in the shallow part of the fault along the trench in this study are nearly the same as their results (the maximum slip of about 30 m).

The time progression of the rupture shows that the source process of the earthquake consists of 3 rupture stages. In order to explain the contributions to the waveforms in the three stages, we divided the source model into Areas 1, 2 and 3: the deeper part of the fault, the shallower asperity area of the northern part of the fault, and the southern part of the fault. In the first stage of the fault rupture, moderate moment-rate areas are found at the southern and deeper side of the rupture starting point (the frame of 15–30 s). The rupture front also reached the shallower part of the fault (asperity area) at about 40 s after the rupture initiation, and rupture progression seems to be suspended in that part. At

45–60 s after the rupture initiation, the second stage of the rupture started in the shallower part of the fault. The asperity area, with a length of about 300 km, simultaneously began to rupture with a high moment rate, and the rupture continued for 30–40 s (the frames of 45–60 s to 75–90 s). Moderate moment was released in the deeper part of the fault (the frame of 75–90 s). After the moment rate in the asperity area declined, the third stage of the rupture seemed to be triggered. After that, the rupture mainly progressed to the southern part of the fault (the frame of 90–105 s), and the deeper part of the fault (the frames after 105–120 s). In the frames of 90–105 s and 105–120 s, some moderate moment-rate areas in the southern part of the fault plane are recognized. The rupture of these areas radiated short-period motions with a short pulse width of moment-rate functions corresponding to strong motion generation area described in the next section.

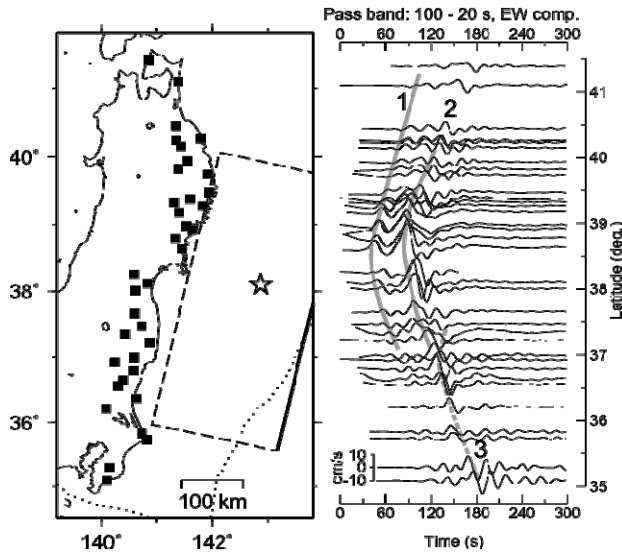


Fig. 1. (Left) Map showing F-net and KiK-net stations (solid square) and the assumed fault plane (rectangle). The star shows the epicenter determined by JMA. (Right) Band-pass filtered velocity seismograms of the horizontal EW component. Pass-bands are 0.01–0.05 Hz (100–20 s). The waveforms are pasted up with the delay time from the origin time.

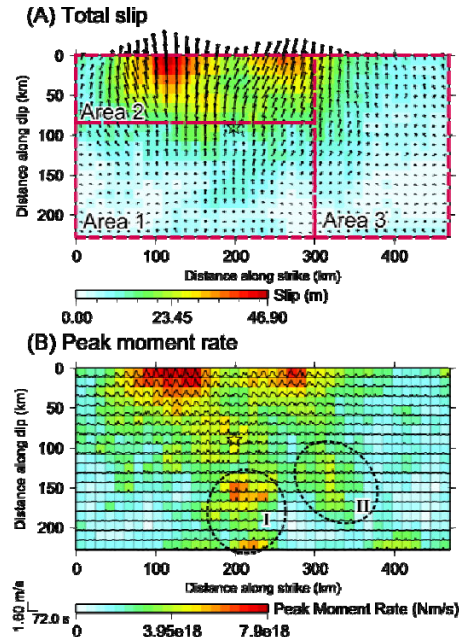


Fig. 2. Upper: Distributions of coseismic slip obtained for the 2011 Tohoku Earthquake. The star indicates the rupture starting point. The rectangle represented by the dashed line indicates 3 areas, Area 1, 2, and 3 denoted in the text. Lower: Distributions of peak moment rate together with the slip rate function at each subfault.

SHORT-PERIOD SOURCE MODEL

Locations of strong motion generation areas

Based on the aftershock distribution in the first 24 hours and the CMT solution by Japan Meteorological Agency (JMA), we define the source fault as roughly 450 km long and 200 km wide with strike of 193° and dip 10° . The hypocenter is at 38.1033° N, 142.86° E, and 23.7 km deep by JMA. The locations of the SMGAs are constrained using the back-propagation method of Kurahashi and Irikura (2010). The acceleration records at stations along a line from north to south are arranged with the same time and amplitude scale in Fig. 3. In the aligned records several isolated wave-packets are found arriving from different origins on the source fault. Such origins are considered to be the strong motion generation areas (SGMAs).

We identified five wave-packets in the observed seismograms, which originate from five SMGAs on the source fault. The onsets of the wave-packets are found to propagate with a certain velocity as shown in Fig. 3. We can estimate the locations of the SMGAs based on the onset times of the

wave-packets at many stations. The origin of each wave-packet, that is the starting point of each SMGA, is theoretically determined on the source fault from the arrival times at more than three stations by the back-propagation method taking the coordinates (x, y, and z) and rupture velocity V_r as variables and assuming unbounded media with constant S wave velocity V_s (Kurahashi and Irikura, 2010). However, for the Tohoku earthquake, strong motion data exist only on the west side of the source fault. Therefore, the initiation of each SMGA cannot be isolated at a point, but rather it is blurred along an area about 20 km in length due to the poor spatial coverage of the observation sites. After estimating the approximate location of each SMGA by the back-propagation method, we calculate ground motions from the SMGA assuming its area (length x width) and initiation point. Then we obtain the final solutions for the area and initiation point by comparing the observed seismograms of each wave-packet and the synthetic ones at many stations using a trial and error approach. The fitting function is adopted to minimize the sum of residuals for acceleration envelopes and velocity waveforms between the observed and synthetic ones.

Characterized source model and ground motion simulation

To calculate ground motions from each SMGA, the area of the SMGA is divided into equal-sized square subfaults, the area of which is set to be the same as the small event area. The rise time and rupture velocity inside each SMGA are given to be $W_s/4V_r$ (W_s : width of the SMGA and V_r : rupture velocity) following empirical relations by Kataoka et al. (2003). The average S wave velocity is given to be 3.5 km/s from T_s -p time versus arrival time at observed stations. The rupture velocities outside of the SMGAs are estimated by the back-propagation method. The total ground motion response at each station is calculated by summing the contributions from the SMGAs with the arrival times from the initiation points of the SMGAs to the station.

The small events' records used as empirical Green's functions (EGFs) have to share the propagation-path and site effects as well as the radiation characteristic from the source. Therefore, the records from the small events (closed star marks in Fig. 4) occurring near the SMGAs are adopted as the EGFs. The records from Event A are used as the EGFs for SMGA 1, SMGA 2, and SMGA 3 because those SMGAs are located close to each other on the preliminary analysis. Those from Event B and Event C are used for SMGA 4 and SMGA 5 offshore Fukushima prefecture and offshore Ibaragi prefecture, respectively. The source information of the mainshock and the small events for the EGFs is listed in Table 1.

Table 1. The source parameters of the mainshock and small events A, B, and C.

	Origin time	Latitude (deg)	Longitude (deg)	Mw	strike (deg)	dip (deg)	rake (deg)				
Mainshock	2011/3/11 14:46	38.103	142.86	9.0	24/193	81/10	92/79				

	Origin time	Latitude (deg)	Longitude (deg)	Mw	strike (deg)	dip (deg)	rake (deg)	Mo (Nm)	corner frequency (Hz)	Stress Drop (MPa)	Area (km ²)
Event A	2011/3/10 6:24	38.172	143.045	6.5	22/213	68/23	85/101	5.51E+18	0.22	11.8	108.9
Event B	2007/11/26 22:51	37.304	141.757	5.9	24/217	71/20	86/102	7.66E+17	0.3	4.1	58.5
Event C	2009/2/1 6:52	36.717	141.279	5.7	25/232	76/15	83/116	4.65E+17	0.48	10.4	22.9

The characterized source model consisting of five SMGAs is obtained by minimizing the fitting function as described in the previous section. The area and initiation of each SMGA are shown in Fig. 4 by a rectangle and closed circle mark, respectively. The source parameters of the final source model, such as the length, width, seismic moment, stress drop and delay time from the origin time of each SMGA are listed in Table 2. The observed and synthetic ground motions at IWTH27 and MYGH04, from the final source model are shown in Fig. 5. The agreement between the observed and synthetic ones is satisfactory at almost all of stations, although the comparison was shown at only two stations.

SMGA 1 is located in the source region of Southern Sanriku-oki west of the hypocenter and SMGA 2 in that of the Middle Sanriku-oki north of the hypocenter. SMGA3 is located in the source

region of the Miyagi-oki, SMGA 4 is located in that of Fukushima-oki and SMGA 5 is located in that of Ibaraki-oki. SMGA 1, SMGA 2, SMGA 3, SMGA 4, and SMGA 5 initiated to rupture 15.6 sec, 66.4 sec, 68.4 sec, 109.7 sec, and 118.2 sec after the rupture originated at the hypocenter. The probabilities of earthquake occurrence in these source regions including the five SMGAs have been estimated by the ERC at less than 7 % to 99 % with magnitude about 6.9 to 7.5, separately.

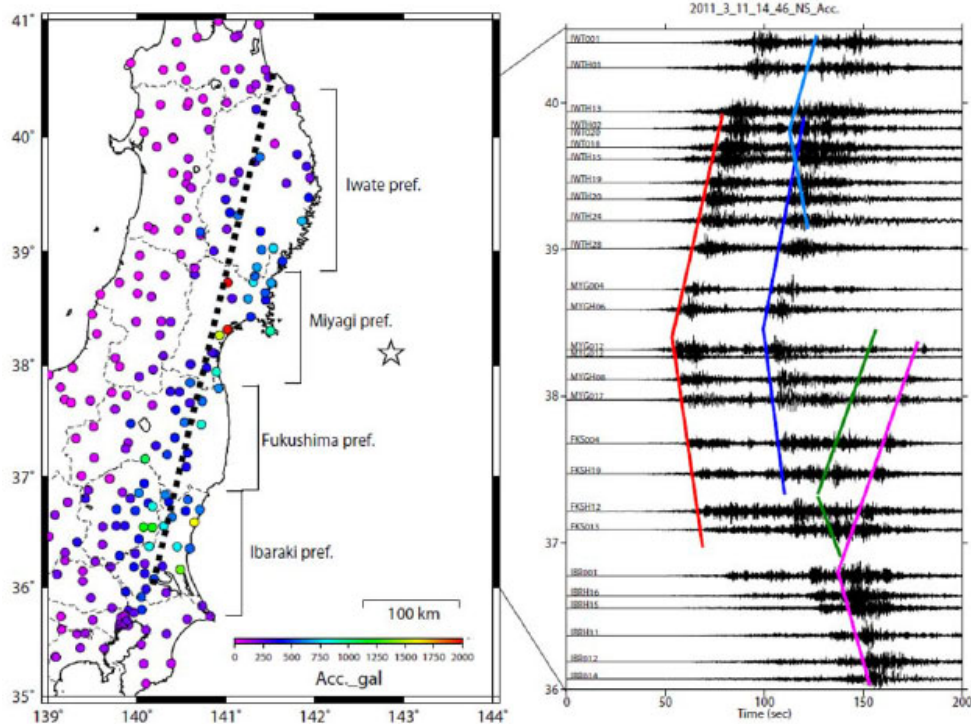


Fig.3. Left: Map showing the location of observed stations. Right: Acceleration seismograms at stations along a line from north to south. The colored thin solid lines indicate the travel times of S waves generated from five strong-motion-generation-areas. Red, sky-blue, blue, green and pink are for the S waves propagating from SMGA 1, SMGA 2, SMGA 3, SMGA 4 and SMGA 5 to the stations, respectively.

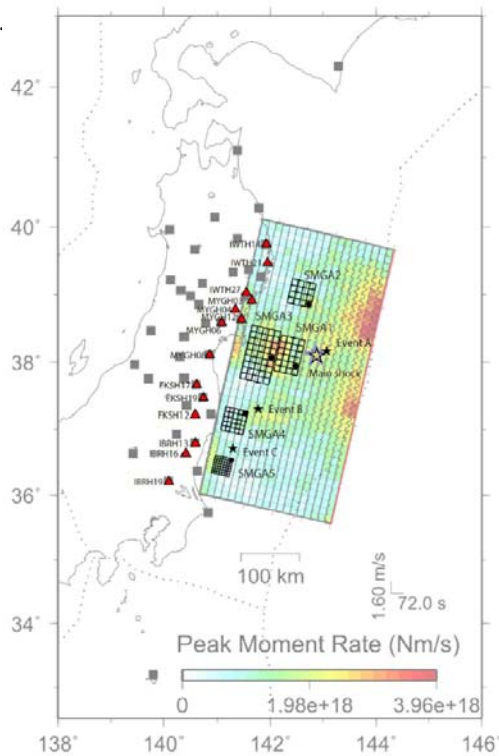


Fig.4. Source model consisting of five SMGAs. The five SMGAs are superposed on the distribution of peak moment-rate inverted using strong motions data by Yoshida et.al. (2011). The initiation point at each SMGA is roughly estimated by the back-propagating method. The area, stress drop and initiation point of each SMGA are estimated from the forward modeling comparing the observed and synthetic ones using the empirical Green's function method. The open star and closed stars show the epicenters of the mainshock and small events A, B, and C, respectively. The small rectangles and closed circles inside them show the SMGAs and their initiation points. The closed red triangles indicate the KiK-net stations used for analysis.

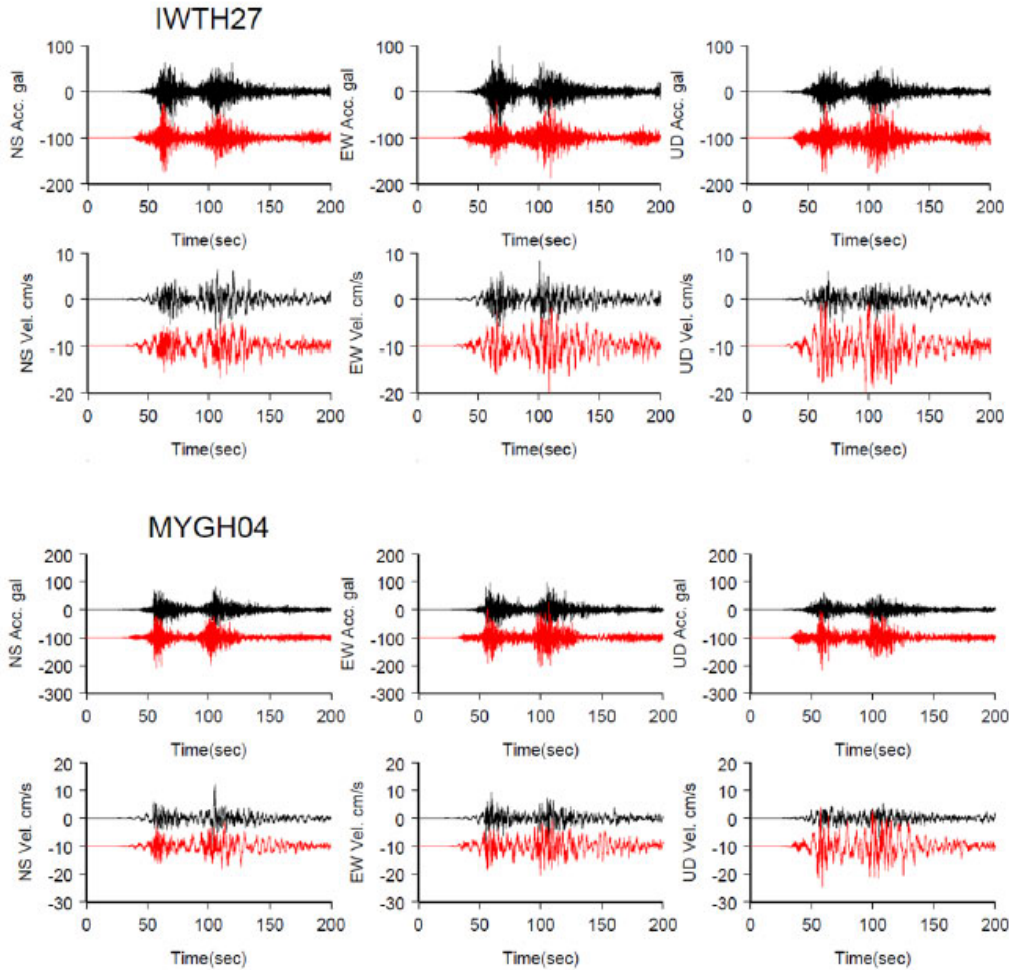


Fig. 5. Comparison of the observed (black lines) and synthetic (red lines) seismograms by the empirical Green's function method at IWTH27 and MYGH04. The acceleration (upper) and velocity (lower) at each station are compared.

FEATURES OF STRONG GROUND MOTIONS

The horizontal components of peak ground velocity (PGV) and those of peak ground acceleration (PGA) observed during this earthquake were compared with empirical attenuation relationships (i.e. strong motion prediction equation) for Mw 7 to Mw 9 by Si and Midorikawa (1999) as shown in Fig. 6. Very limited data of PGV and PGA for earthquakes with more than Mw 8 and no data for Mw 9 earthquake were used to make the empirical equation by them. Therefore, the attenuation relationship for Mw 9 is just extrapolation of the equation by Si and Midorikawa (1999).

We found that the attenuation-distance relationship of the peak ground velocity (PGV) from this earthquake was virtually equivalent to the empirical one from an earthquake of Mw 8.0. On the other hand, peak ground acceleration (PGA) was also virtually equivalent to the empirical one from Mw 8.0 in the distance over 100 km, but clearly larger than that from Mw 8.0 near the source fault.

High Accelerations were mainly caused by two different mechanisms.

A: Ground motions with extremely high acceleration more than 1000 gals were recorded at soft grounds formed by the Quaternary deposits. Extremely high accelerations were generated by large amplifications due to surface geology with decreased S wave velocities (nonlinear soil behavior).

B: Ground motions with relatively high acceleration caused by source characteristics, such as rupture directivity effects, heterogeneous slip velocity inside the strong motion generation areas and so on.

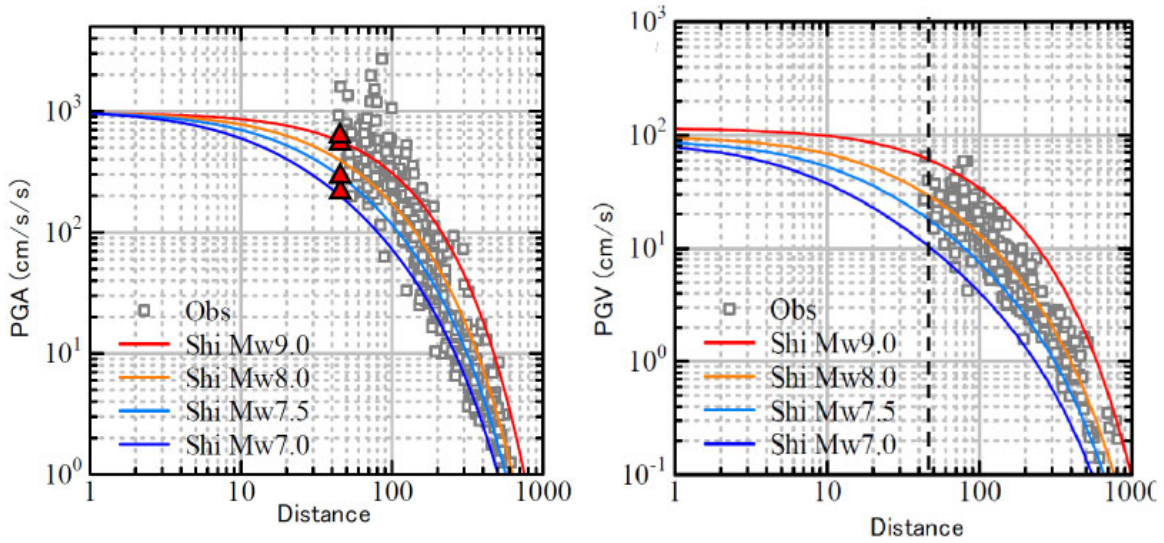


Fig. 6. Comparison of Observed Data of PGA and PGV from the 2011 Tohoku earthquake (Mw 9.0) with and the empirical attenuation-distance relationships for Mw 7.0 to Mw 9.0 by Shi and Midorikawa (1999). Right is for PGA and left is for PGV.

On a map in the left of Fig. 7, stations are shown where high accelerations caused by A were recorded. The observed accelerations there seem to be remarkably deviated from the attenuation-distance curves as shown in the right figure of Fig. 7. We found those stations were put on soft grounds formed by the Quaternary deposits grounds. Examples of acceleration waveforms at those stations are shown in Figure 8. Their waveforms present clear cyclic mobility.

We examined site responses at the K-NET Tsukidate (MYG004) where the largest PGA, 2933 gals, was recorded. H/V spectral ratio during the mainshock is compared with that for weak motions as shown in Fig. 9. The site response for weak motions is taken as average of the H/V during small earthquakes. The predominant period of the site responses at Tsukidate during the mainshock is clearly shifting to longer than that during weak motions, showing reduction of S wave velocity in near-surface layers. However, there was very little damage during this earthquake in the vicinity of the Tsukidate station. It is caused by the predominant period of ground shaking shorter than 0.5 second, although accelerations were so high.

We found that spectral characteristics of ground motions have predominant periods shorter than 0.5 at most of places where high accelerations were recorded. It might be explained by predominant periods shorter than 1 sec that there were relatively small damage of houses and buildings due to ground shakings.

Ground motions with relatively high acceleration caused by source characteristics, i.e. B, are simulated assuming a source model with heterogeneous slip velocity inside a SMGA. This model is similar to super-asperity model proposed by Matsushima and Kawase (2006) and frequency-dependent asperity model by Miyake and Koketsu (2010). Ground motions at ONG128 (Onagawa NPP), one of nearest station to the source fault, were simulated, using the new model with heterogeneous slip velocity inside SMGA3. We can see that simulated acceleration and velocity waveforms by the new model agree well with observed waveforms, compared with simulated ones by conventional model as shown in Fig. 10.

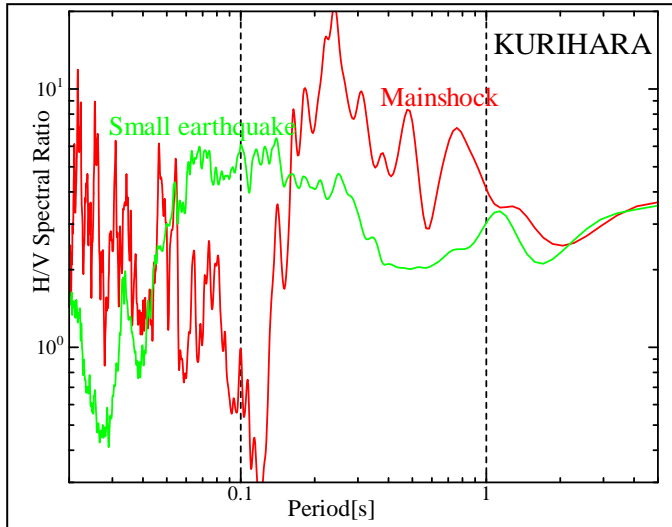


Fig. 9. Site responses at the K-NET Tsukidate (MYG004) where the largest PGA, 2933 gals. H/V spectral ratios during the mainshock (red) is compared with that for weak motions (green). The site response for weak motions is taken as average of the H/V during small earthquakes.

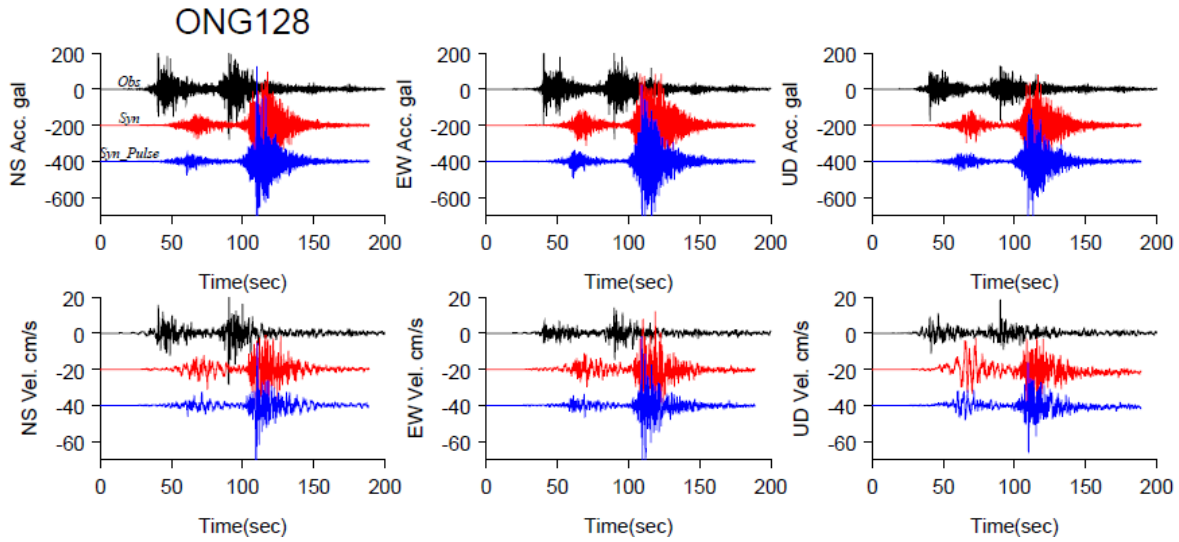


Fig. 10. Ground motions at ONG128 (Onagawa NPP), one of nearest station to the source fault, were simulated, using the new model with heterogeneous slip velocity inside SMGA3.

CONCLUSIONS

The source model inverted from long period ground motion data (20 to 200 sec) by Yoshida et al. (2012) shows that a large asperity (about 300 km \times 100 km) located on the shallower part of the fault was estimated, and maximum slip is about 47 m. This source model with a shallow large asperity is consistent with the tsunami source model (Fujii and Satake, 2011).

We find that acceleration as well as velocity motions during the 11 March 2011 off Tohoku, Japan earthquake (Mw 9.0) are well simulated using a characterized source model consisting of five SMGAs. SMGA 1 is located in the source region of Southern Sanriku-oki west of the hypocenter and SMGA 2 in that of the Middle Sanriku-oki north of the hypocenter. SMGA3 is located in the source region of the Miyagi-oki, SMGA 4 is located in that of Fukushima-oki and SMGA 5 is located in that of Ibaraki-oki. SMGA 1, SMGA 2, SMGA 3, SMGA 4, and SMGA 5 initiated to rupture 15.6 sec, 66.4 sec, 68.4 sec, 109.7 sec, and 118.2 sec after the rupture originated at the hypocenter. The probabilities of earthquake occurrence in these source regions including the five SMGAs have been estimated by

the ERC at less than 7 % to 99 % with magnitude about 6.9 to 7.5, separately.

The locations of the SMGAs coincide with large peak moment-rate areas inverted from long period ground motion data (20 – 200 sec) by Yoshida et al. (2011), particularly along the down-dip edge of the source fault.

Attenuation-distance relationship of peak ground velocity (PGV) from this earthquake was virtually equivalent to the empirical one from Mw 8.0 determined by Si and Modorikawa (1999). On the other hand, peak ground acceleration (PGA) was also virtually equivalent to the empirical one from Mw 8.0 in the distance over 100 km, but clearly larger than that from Mw 8.0 near the source fault.

Ground motions with extremely high-accelerations cannot be simulated near the source fault using the source model mentioned above. Then, two different mechanisms for Group A and B are examined for explaining such high accelerations. A: Ground motions with extremely high acceleration more than 1000 gals were recorded at soft grounds formed by the Quaternary deposits. Extremely high accelerations were generated by large amplifications due to surface geology with decreased S wave velocities (nonlinear soil behavior). B: Ground motions with relatively high acceleration were generated by heterogeneous slip velocity inside the strong motion generation areas. That is, stress parameters are not uniform inside the strong motion generation areas.

ACKNOWLEDGMENTS

We used the wave data provided by the KiK-net of National Research Institute for Earth Science and Disaster Prevention (NIED). We also used the hypocentral information from Japan Meteorological Agency, and the moment tensor solution from the F-net (NIED). The long-period source model was referred from Yoshida, Miyakoshi, and Irikura (2011).

REFERENCES

- Kawashima, K. (1995a). “Dynamic response analysis of structures.” *Journal of Earthquake Engineering*, Vol. 3, No. 2, 213-222.
- Kawashima, K. (1995b). “Seismic damage in the past earthquakes.” *Journal of Earthquake Engineering*, Vol. 7, No. 3, 151-159.
- Priesley, M. J. N., Seible, F. and Calvi, G. M. (1996). “*Seismic design and retrofit of bridges*.” Wiley Interscience Publications, New York, USA.
- Vesic, A. (1961). “Beams on elastic foundation.” *Proc. 5th International Conference on Soil Mechanics and Foundation Engineering*, Vol. 1, 845-850.
- Bouchon, M. (1981). A simple method to calculate Green’s functions for elastic layered media”, *Bull. Seismol. Soc. Am.*, **71**, 959–971.
- Earthquake Research Committee (2005). “Long-term forecast of earthquakes from Sanriku-oki to Boso-oki (revised) (in Japanese)”, 80 pp., Headquarters for Earthquake Research Promotion.
- Earthquake Research Committee (2011). “The 2011 off the Pacific Coast of Tohoku Earthquake”, <http://www.jishin.go.jp/main/index-e.html>.
- Fujii, Y. and K. Satake (2011). Off Tohoku-Pacific Tsunami on March 11, 2011, <http://iisee.kenken.go.jp/staff/fujii/OffTohokuPacific2011/tsunami.html>.
- Hartzell, S. H. and T. H. Heaton (1983). Inversion of strong ground motion and teleseismic waveform data for the fault rupture history of the 1979 Imperial Valley, California, earthquake, *Bull. Seismol. Soc. Am.*, **73**, 1553–1583.
- Hoshiba1, H., Iwakiri, K., Hayashimoto, N., Shimoyama, T., Hirano, K., Yamada, Y., Ishigaki, Y., and Kikuta, H. (2011). “Outline of the 2011 off the Pacific coast of Tohoku Earthquake (Mw 9.0) —Earthquake EarlyWarning and observed seismic intensity—”, *Earth Planets Space*, **63**, 547–551.
- Ide, S., A. Baltay, and G. Beroza (2011). Shallow dynamic overshoot and energetic deep rupture in the 2011 Mw 9.0 Tohoku-oki earthquake, *Science*, doi:10.1126/science.1207020.
- Iinuma, T., M. Ohzono, Y. Ohta, and S. Miura (2011). Coseismic slip distribution of the 2011 Off the

- Pacific Coast of Tohoku Earthquake estimated based on GPS data, Japan Geoscience Union Meeting 2011, MIS036-P22.
- Irikura, K. (1986). Prediction of strong acceleration motions using empirical Green's function, *Proc. 7th Japan Earthq. Eng. Symp.*, 151–156.
- Kataoka, S., K. Takaaki, M. Jun, and T. Keiichi (2003). Study on a Procedure for Formulating Level 2 Earthquake Motion Based on Scenario Earthquakes, RESEARCH REPORT of National Institute for Land and Infrastructure Management, No.15.
- Kennet, B. L. N. and N. J. Kerry (1979). "Seismic waves in a stratified half space", *Geophys. J. R. Astron. Soc.*, **57**, 557–583.
- Koketsu K., Yokota Y., Nishimura N., Yagi Y., Miyazaki S., Satake K., Fujii Y., Miyake H., Sakai S., Yamanaka Y., Okada T. (2011). "A unified source model for the 2011 Tohoku earthquake", *Earth and Planetary Science Letter*, **310**, 480–487.
- Kurahashi, S. and K. Irikura (2010). "Characterized Source Model for Simulating Strong Ground Motions during the 2008 Wenchuan Earthquake", *Bull. Seism. Soc. Am.*, **100**, 2450–2475.
- Kurahashi, S. and K. Irikura (2011), "Source model for generating strong ground motions during the 2011 off the Pacific coast of Tohoku Earthquake", *Earth Planets Space*, **63**, 571–576.
- Matsushima, S. and H. Kawase (2006). Proposal of super-asperity model for subduction earthquakes, *Monthly Chikyū*, No.55, 98-102.
- Miyake, H., and K. Koketsu (2010). Testing the double corner source spectral model for long- and short-period ground motion simulations, 2010 AGU Fall Meeting, Abstract S53D-05.
- Muramatsu, I., T. Sasatani, and I. Yokoi (2001). "Velocity-type strong-motion seismometer using a coupled pendulum: Design and performance", *Bull. Seismol. Soc. Am.*, **91**, 604–616.
- National Institute of Earth Sciences and Disaster Prevention (2011). 2011 Off the Pacific Coast of Tohoku earthquake, Strong Ground Motion, http://www.k-net.bosai.go.jp/k-net/topics/TohokuTaiheiyo_20110311/nied_kyoshin2e.pdf, March 13.
- Ozawa, S., T. Nishimura, H. Suito, T. Kobayashi, M. Tobita, and T. Imakiire (2011), coseismic and postseismic slip of the 2011 magnitude-9 Tohoku-Oki earthquake, *Nature*, **475**, 373–376.
- Sasatani, T., T. Maeda, K. Yoshida, N. Morikawa, M. Ichianagi, Y. Motoya, and M. Kasahara (2002). "Strong-motion Observation in Hokkaido with Broadband, Velocity-type Seismometers", *Geophys. Bull. Hokkaido Univ.*, **65**, 335–345.
- Somerville, P., K. Irikura, R. Graves, S. Sawada, D. Wald, N. Abrahamson, Y Iwasaki, T Kagawa, N. Smith, and A. Kowada (1999). Characterizing crustal earthquake slip models for the prediction of strong ground motion, *Seism. Res. Lett.* **70**, 59-80.
- Smith, A. (2011). Focal mechanism of the 2011 off the Pacific coast of Tohoku Earthquake, *Earthquake Planets Space*.
- Wu, C., K. Koketsu, and H. Miyake (2008), "Source processes of the 1978 and 2005 Miyagi-oki, Japan, earthquakes: Repeated rupture of asperities over successive large earthquakes", *J. Geophys. Res.*, **113**, B08316.
- Wu, C., K. Koketsu, and H. Miyake (2009). "Correction to "Source processes of the 1978 and 2005 Miyagi-oki, Japan, earthquakes: Repeated rupture of asperities over successive large earthquakes", *J. Geophys. Res.*, **113**, B08316, 2009.
- Yagi, Y. and N. Nishimura (2011). The Mar 11, 2011 Tohoku-Pacific Coast Earthquake (Ver. 3), <http://www.geol.tsukuba.ac.jp/~yagi-y/EQ/Tohoku/>
- Yamanaka, Y. (2011). The March 11, 2011 Off the Pacific Coast of Tohoku earthquake, http://www.seis.nagoya-u.ac.jp/sanchu/Seismo_Note/2011/NGY36n.html.
- Yokota, Y., Koketsu, K., Fujii, Y., Satake, K., Sakai, S., Shinohara, M., and Kanazawa, T. (2011). "Joint inversion of strong motion, teleseismic, geodetic, and tsunami datasets for the rupture process of the 2011 Tohoku earthquake", *Geophys.Res.Lett.*, **38**, L00G21, 5 PP., doi:10.1029/2011GL050098.
- Yoshida, K., K. Miyakoshi, and K. Irikura (2011). Source Process of the 2011 Tohoku Earthquake Inferred from Weaveform Inversion with Long-Period Strong-Motion Records, *Earth Planets Space*, **63**, 577-582.